CHEMISTRY OF MATERIALS
Cite This: Chem. Mater. 2018, 30, 1776−1781
Article
pubs.acs.org/cm

Arrhenius Behavior of the Bulk Na-Ion Conductivity in $Na_3Sc_2(PO_4)_3$ Single Crystals Observed by Microcontact Impedance Spectroscopy

Daniel Rettenwander,*[,†,‡] Günther J. Redhammer,[§] Marie Guin,[⊥,¶] Artur Benisek,[§] Hannes Krüger,[#] Olivier Guillon,[¶] Martin Wilkening,[†,‡] Frank Tietz,[⊥,¶] and Jürgen Fleig[∥]

[†]Institute of Chemistry and Technology of Materials and [‡]Christian Doppler Laboratory for Lithium Batteries, Institute for Chemistry and Technology of Materials, Graz University of Technology, 8010 Graz, Austria

[§]Department of Chemistry and Physics of Materials, University of Salzburg, 5020 Salzburg, Austria

[⊥]Institute of Energy and Climate Research, Materials Synthesis and Processing (IEK-1), Forschungszentrum Jülich GmbH, 52425 Jülich, Germany

[¶]Helmholtz-Institute Münster, c/o Forschungszentrum Jülich GmbH, 48149 Jülich, Germany

[#]Institute of Mineralogy and Petrography, University of Innsbruck, 6020 Innsbruck, Austria

[∥]Institute for Chemical Technologies and Analytics, Vienna University of Technology, 1060 Vienna, Austria

ABSTRACT: NASICON-based solid electrolytes with exceptionally high Na-ion conductivities are considered to enable future all solid-state Na-ion battery technologies. Despite 40 years of research the interrelation between crystal structure and Na-ion conduction is still controversially discussed and far from being fully understood. In this study, microcontact impedance spectroscopy combined with single crystal X-ray diffraction, and differential scanning calorimetry is applied to tackle the question how bulk Na-ion conductivity σ_{bulk} of sub-mm-sized flux grown $Na_3Sc_2(PO_4)_3$ (NSP) single crystals is influenced by supposed phase changes (α, β, and γ phase) discussed in literature. Although we found a smooth structural change at around 140 °C, which we assign to the $\beta \rightarrow \gamma$ phase transition, our conductivity data follow a single Arrhenius law from room temperature (RT) up to 220 °C. Obviously, the structural change, being mainly related to decreasing Na-ion ordering with increasing temperature, does not cause any jumps in Na-ion conductivity or any discontinuities in activation energies E_a. Bulk ion dynamics in NSP have so far rarely been documented; here, under ambient conditions, σ_{bulk} turned out to be as high as 3×10^{-4} S cm^{-1} at RT ($E_{a,\,bulk}$ = 0.39 eV) when directly measured with microcontacts for individual small single crystals.

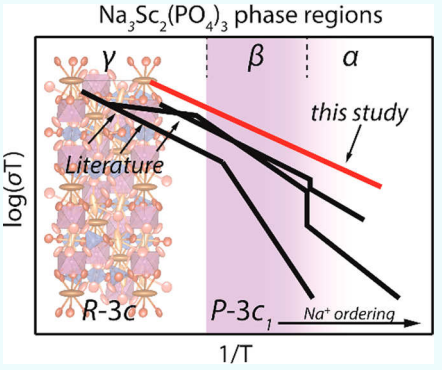

INTRODUCTION

Li-ion conducting solid electrolytes are highly desired for new battery concepts overcoming serious safety issues of state-of-the-art battery technologies using liquid-based electrolytes. Moreover, the use of solid electrolytes enables very high energy densities as well as chemical and electrochemical stability, which is needed for any automotive and grid storage applications. Concerns regarding the availability of mineral resources of Li, however, increase the interest in other cations such as Na. Among Na-ion conducting solid electrolytes, NASICON-based materials, with the formula $Na_nM_2(XO_4)_3$ (M = Sc, Zr, etc.; X = Si^{4+}, P^{5+}, etc.), are considered as one of the most promising candidates for future all solid-state Na-ion battery (ASSNIB) technologies. These solid electrolytes were discovered by Hong et al. about 40 years ago described with the rhombohedral space group (*SG*) $R\bar{3}c$, known as the NASICON structure.[1,2]

The structural situation in this class of material is, however, rather complicated and still not fully understood. As an example, in the case of $Na_3V_2(PO_4)_3$ (NVP) a phase transition sequence from an ordered monoclinic α form (space group (SG) C2/*c*, *a* = 15.1244(6) Å, *b* = 8.7287(3) Å, *c* = 21.6143(8) Å, β = 90.163(2)) to the classical disordered rhombohedral cell (*SG* $R\bar{3}c$, *a* = 8.73382(4) Å, *c* = 21.91438(17) Å) with two intermediate incommensurate modulated structures β and β' was described.[3] A further complication arises due to the different and conflicting behavior of powders and single crystals of NASICON-materials.[4] For polycrystalline samples of $Na_3Sc_2(PO_4)_3$ (NSP), fabricated at high temperatures, two phase transitions are reported[5−7] with the room temperature (RT) structure often being described using a monoclinic cell with space group symmetry C2/*c*.[8−11] In contrast, flux grown single crystals are reported to show only a single phase transition at around 160 °C from the high temperature structure with *SG* $R\bar{3}c$ to a more complicated trigonal structure with a 2*a*, *c* supercell.[4,12,13]

It has been reported that these structural changes in NASICON materials are associated with changes of the thermal

Received: January 14, 2018
Revised: February 22, 2018
Published: February 22, 2018

DOI: 10.1021/acs.chemmater.8b00179
Chem. Mater. 2018, 30, 1776−1781

activation of Na-ion conductivity. While for NSP in some papers only a single change in activation energy (E_a) associated with the $\alpha \rightarrow \beta$ or $\beta \rightarrow \gamma$ phase transition is detected, in other papers, however, two changes in Na-ion conductivity were reported and assigned to the two structural changes. Some of these discrepancies in structure−property relationships published in literature seem to be related to the use of total Na-ion conductivities instead of bulk Na-ion conductivities. The total conductivity comprises both grain boundary and bulk contributions. Of course, only the latter contains intrinsic transport properties which, to our opinion, will be mostly affected by the crystal chemical changes. Hence, with the data available until now, the apparently observed jumps in the thermal activation of the conductivity cannot be unequivocally assigned to the phase transitions reported.

Extremely high bulk conductivities in the mS cm^{-1} range are equivalent to electrical relaxation processes with very short relaxation times. At ambient or slightly elevated temperature, the relaxation frequencies of these low resistive bulk processes with capacitances in the pF range are only seen in the MHz to GHz regime. If powder samples are examined, the presence of grain boundaries often complicates the evaluation of impedance data in Nyquist plots and may hinder an unambiguous analysis of the bulk conductivity. Moreover, chemical and structural inhomogeneities in polycrystalline samples may limit the accurate study of electrochemical properties as only mean values are accessible. The use of microelectrodes on top of single crystals, however, enables a very precise study of conductivity properties since the obtained electrochemical data usually only depend on electrical bulk properties and morphology. Therefore, they can directly be correlated with information from single crystal diffraction. Very recently, we used the same setup with microelectrodes to successfully investigate electrical bulk properties of $Li_{1+x}Al_xTi_{2-x}(PO_4)_3$ (LATP) single crystals.[14]

Here, microcontact impedance spectroscopy (MC IS) is combined with single crystal X-ray diffraction (SC XRD) to study possible interrelationships between intragrain Na-ion conductivity and phase transitions of flux grown NSP single crystals. Surprisingly, contrary to the various reports in literature, we do not observe any discontinuities in Na-ion conductivity as a function of temperature.

EXPERIMENTAL SECTION

Synthesis of Single Crystals. Single crystals of $Na_3Sc_2(PO_4)_3$ were grown using the flux method as described by Sotofte and Fu.[15] First, $ScPO_4$ was prepared via solid state reaction from a stoichiometric amount of Sc_2O_3 (Projector GmbH, 99.5%) and $NH_4H_2PO_4$ (Merck KGaA, 99%). The homogenized mixture was heated up with 300 K/h to 900 °C for 3 h. After grinding, the powder was annealed at 1200 °C for 20 h. A ratio 1:6 of $ScPO_4$ and Na_4P_2O7 (Sigma-Aldrich, 95%) was heated in a Pt crucible at 1100 °C for 5 h in air, then cooled down to 900 °C at 3 K/h, before the furnace was free cooled to RT. The single crystals of several hundreds of μm in size were extracted from the molten mass with hot water.

Single Crystal X-ray Diffraction. SC XRD data at RT were collected on several crystals on a Bruker SMART APEX CCD-diffractometer. Intensity data were collected with graphite-monochromatized Mo K_α X-ray radiation (50 kV, 30 mA). The crystal-to-detector distance was 30 mm and the detector positioned at −28° 2Θ using an ω-scan mode strategy at four different ϕ positions (0°, 90°, 180°, and 270°). 630 frames with $\Delta\omega = 0.3°$ were acquired for each run. Three-dimensional data were integrated and corrected for Lorentz-, polarization, and background effects using the APEX3 software.[16] To study the evolution of the crystal structure with temperature, three data sets (at 298, 403, and 503 K) were also collected at an STOE IPDS II single-crystal diffractometer system equipped with an image plate detector at the University of Innsbruck. Elongated exposure time of 120 s per frame and significantly finer increments of 0.1° were chosen. Intensity integration was performed with X-Area software.[17]

Differential Scanning Calorimetry. The heat capacity between 0 and 300 °C was measured using a power compensated PerkinElmer Diamond Differential scanning calorimetry (DSC) on samples weighing ∼38 mg. The DSC measurements were performed under a flow of Ar gas, with the calorimeter block kept at −20 °C using a PerkinElmer Intracooler. Each measurement consisted of a blank run with empty calorimeter chambers, a calibration, and a sample run, where the samples were placed into the sample chamber of the calorimeter. The heat flow data (difference in heating power between the sample and the reference chamber) were collected at 100 °C temperature intervals consisting of a temperature scan (heating rate of 10 °C/min) and isothermal periods of 3 min before and after the temperature scan. The heat flow versus temperature data from the sample runs were shifted and rotated until the data of the isothermal periods agreed with those of the blank run. A sample-saving method for heat capacity measurements on powders using relaxation calorimetry. The data from the blank run were then subtracted from those of the sample run to give the net heat flow of the sample. For calculating the heat capacity, the net heat flow data were finally divided by the heating rate and the mass of the sample. Each sample run was corrected against a calibration run using a synthetic single crystal of corundum (31.764 mg), whose heat capacities were taken from the National Bureau of Standards Certificate.[18] The accuracy of the DSC heat capacity data was determined to be better than 0.6%.

Application of Microelectrodes on Single Crystals. For electrochemical characterization, single crystals were embedded in epoxy resin. Pt thin films were sputter deposited with a thickness of 200 nm on top of approximately 10 nm Ti (used to improve the adhesion between the sample and the electrode). Afterward a negative photoresist was coated on top of the embedded and polished single crystals. After applying the mask with the appropriate microelectrode pattern, in our case circular electrodes with a diameter of 30 μm, the samples were exposed to UV light. Areas that were covered during exposure were removed using a developer solution (Microresist Technologies, Germany). In a subsequent step the microstructure was obtained by ion beam etching.

Microcontact Solid-State Impedance Spectroscopy. The electrochemical characterization of NSP was carried out by electrical impedance spectroscopy according to ref 14. All impedance measurements were performed between RT and 200 °C in a tube furnace using an Alpha-A High Resolution dielectric analyzer with a ZG-2 interface (Novocontrol, Germany) in the frequency range from 3×10^6 Hz to 10^2 Hz with a voltage amplitude of 100 mV. The temperature were measured using a thermocouple placed close to the single crystals. In Figure 1 the microcontact setup and a schematic picture of the performed experiment are shown.

RESULTS

Structural Behavior of NSP Single Crystals as Function of Temperature. In agreement with suggestions presented in literature so far, the RT SC XRD data reveal distinct superstructure reflections and cannot be indexed with a rhombohedral nor with a monoclinic cell.[4,13] This structural complexity was in the very same manner observed for dozens of single crystals, which were tested in the initial phase of our investigation. Figure 2a shows calculations of the precession images from the SC XRD data at different layers at 25 °C, the peaks belonging to the $R\bar{3}c$ cell are marked to highlight the superstructure peaks. The pattern cannot be indexed with the monoclinic cell, frequently encountered in literature for NSP, for example, see Collin et al. (*SG* $C2/c$, $a = 15.404(4)$ Å, $b = 9.103(3)$, $c = 8.919(2)$, $\beta = 123.53$).[13] Also with the enlarged

DOI: 10.1021/acs.chemmater.8b00179
Chem. Mater. 2018, 30, 1776−1781

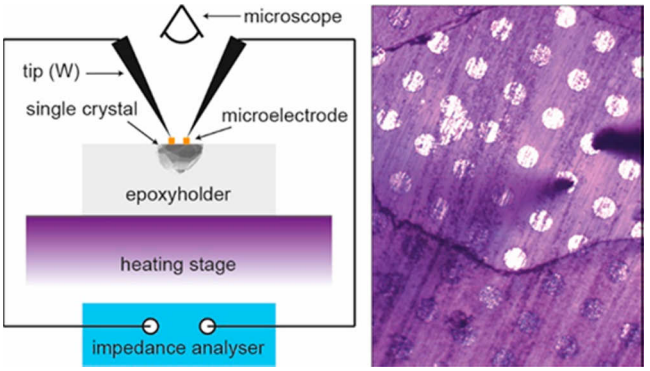

Figure 1. (left) Sketch of the microcontact setup. (right) Enlarged view of an embedded and polished single crystal with patterned electrodes. White areas represent the lithographically prepared Ti/Pt microelectrodes having a diameter of 30 μm. The black triangles are WC needles used to contact the electrodes.

monoclinic cell, recently suggested by Chotard et al. for NVP, it is not possible to index all observed Bragg peaks.[3] The comparison of their reconstructed reciprocal space layer 0*kl* with those of this study reveals substantial differences with the superstructure peaks appearing along the *c** direction; for NVP, they appeared along the *b** direction. The only possibility to index all Bragg peaks for NSP fit with a 2*a*, 2*b*, *c* trigonal cell. The space group is $P\bar{3}c1$, which is a natural subgroup of $R\bar{3}c$ and which is in line with findings of Collin et al. and Tran Qui et al.[12,13]

To monitor possible changes of the crystal structure with temperature, we collected two data sets at elevated temperatures. The data set collected at 130 °C, that is, between the two phase transition temperatures proposed for polycrystalline samples, still shows trigonal symmetry with the only difference of somewhat weaker superstructure reflections.

Importantly, at 230 °C the superstructure has completely vanished and the data can be indexed and refined with the commonly observed $R\bar{3}c$ NASICON structure. Figure 2b shows the reconstructed reciprocal space layer *hk*1 at different temperatures, which clearly shows that the superstructure reflections disappear. The results of the refinements of the high-temperature structure are illustrated in Figure 2c and presented in Table 1.

Table 1. Atomic Coordinates and Equivalent Isotropic Displacement Parameters for NSP Single Crystals at 230 °C[a]

	site	*x*	*y*	*z*	Occ	U_{eq}
Sc1	12c	0	0	1493(1)	1	13(1)
P1	18e	2936(1)	0	2500	1	15(1)
O1	36f	306(3)	2122(2)	1954(1)	1	39(1)
O2	36f	1943(2)	1737(2)	905(1)	1	26(1)
Na1	6b	0	0	0	0.53(1)	161(11)
Na2	18e	6364(3)	0	2500	0.71(1)	81(2)

[a]Atomic coordinates (Å × 10^4); equivalent isotropic displacement parameters (Å^2 × 10^3); U_{eq} is defined as one-third of the trace of the orthogonalized U_{ij} tensor.

At 503 K, the Na(1) site is occupied by ~50%, the Na(2) by ~70%; these estimations give rise to a total Na content of ~2.66 per formula unit (pfu). The structure is characterized by distinct anisotropic motion of the Na atoms. The observation

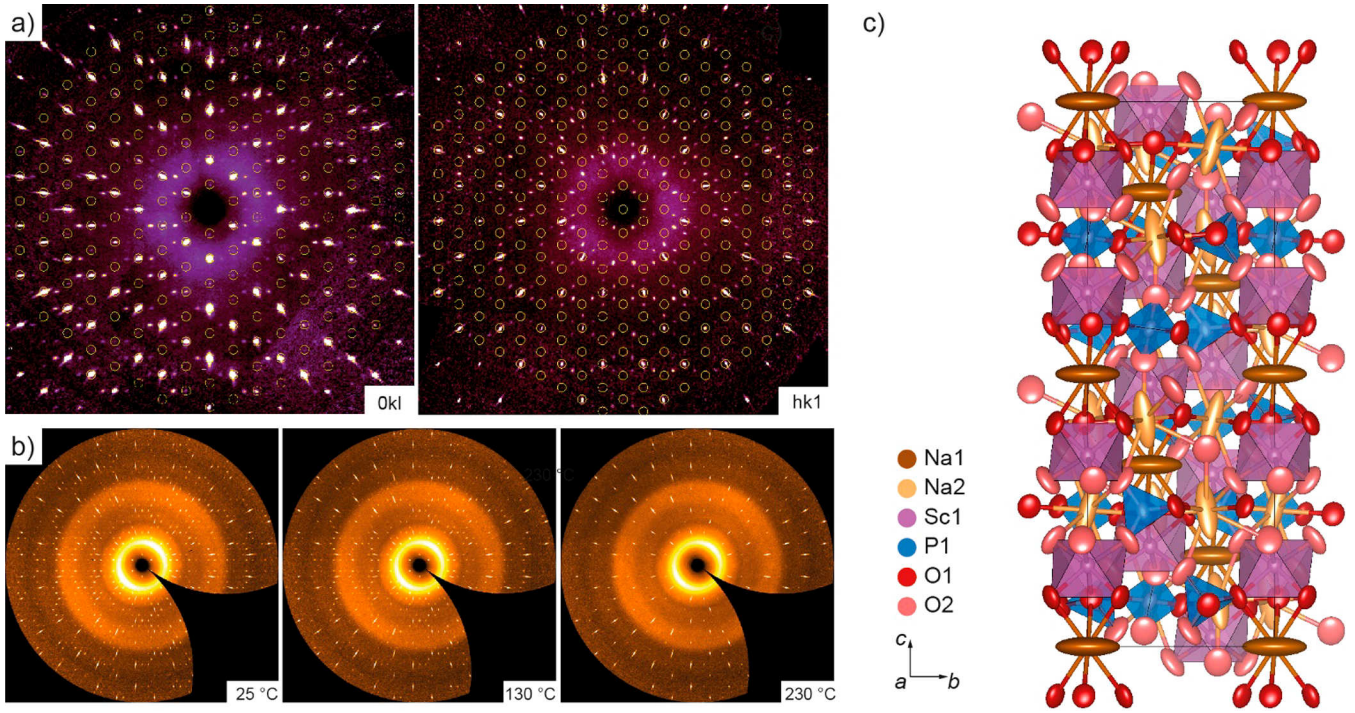

Figure 2. (a) Calculated precession images of the hk1 and 0kl layers in $Na_3Sc_2(PO_4)_3$; the green circles represent the reciprocal lattice point positions of the $R\bar{3}c$ lattice. (b) Calculated precession images of the hk1 layer in $Na_3Sc_2(PO_4)_3$ at different temperatures as extracted from single crystal the X-ray diffraction data using the STOE IPDS-II system. (c) Unit cell (space group $R\bar{3}c$) of $Na_3Sc_2(PO_4)_3$. Dark and bright brownish ellipsoids indicate sodium ions in octahedral sides (Wyckoff position (WP) 6*b* and 18*e*, respectively). Purple octahedral denotes scandium atoms coordinated by oxygen atoms (WP 12*c*). Blue tetrahedral denotes phosphorus atoms coordinated to oxygen atoms (WP 18*e*). Oxygen atoms are located at the corner of the polyhedral (reddish spheres; WP 36*f*).

DOI: 10.1021/acs.chemmater.8b00179
Chem. Mater. 2018, 30, 1776−1781

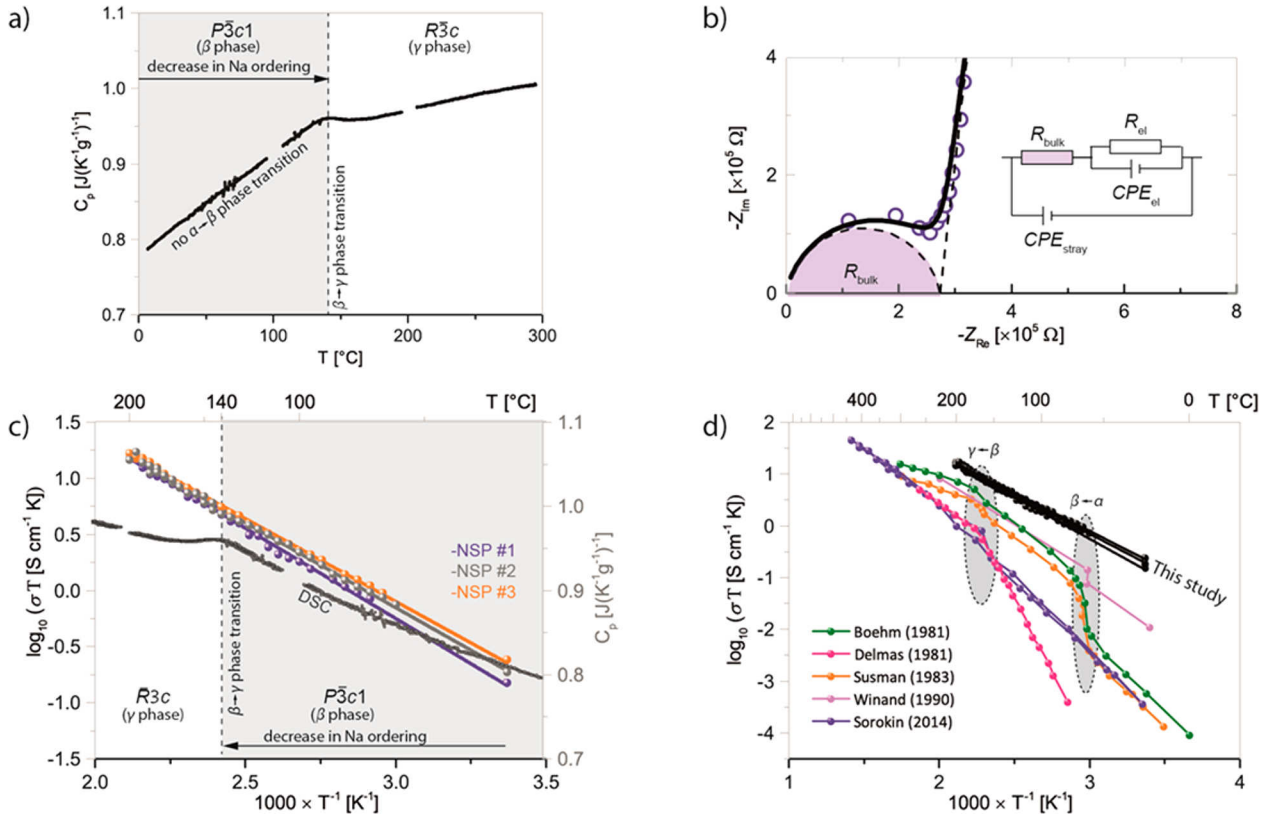

Figure 3. (a) DCS measurement of $Na_3Sc_2(PO_4)_3$ single crystals from 0 to 300 °C. The heat capacity versus temperature data do not show a smooth behavior, but show a peak centered at 140 °C. Although the peak is broad and not very pronounced, it is unmistakably an endothermic peak and can be associated with the $\beta \rightarrow \gamma$ phase transition. (b) Nyquist plot of a representative impedance measurements on $Na_3Sc_2(PO_4)_3$ single crystal measured at 23.5 °C. The equivalent circuit used to approximate the location curve is also shown. While the continuous line represents the total response, the dashed line shows the contributions of the bulk and the electrode. (c) Arrhenius plot of $\sigma_{bulk}T$ of $Na_3Sc_2(PO_4)_3$ single crystals as obtained from micocontact impedance spectroscopy. For comparison, conductivity values extracted from literature are also shown. The $\beta \rightarrow \gamma$ phase transition as observed by DSC is indicated by the vertically drawn line. (d) Arrhenius plot of $Na_3Sc_2(PO_4)_3$ single crystals and value extracted from refs 5 and 19−22. The $\alpha \rightarrow \beta$ and $\beta \rightarrow \gamma$ phase transitions are highlighted in gray.

of the β (most probably $P\bar{3}c1$, see above) to γ ($R\bar{3}c$) phase transition in single crystalline NSP material is further supported by DSC measurements (see Figure 3a), which show a weak and broad peak centered around 140 °C. In strong contrast to the situation reported for powder samples, we found no measurable indications for the α to β phase transition for single crystals.[5] This clear difference might be caused by different synthesis conditions.

To clarify this difference is beyond the scope of the present paper, which focuses on the impact of phase transformations on (bulk) ionic conductivities of NSP single crystals. As the RT structure is yet not complete resolved, no information can be extracted on Na disorder and its influence as a driving force for phase transitions. Symmetry and structural phase transitions of NSP between 100 and 500 K, as well as the role of synthesis conditions, will be presented in a follow-up paper.[19]

Na-Ion Conductivity and Arrhenius Behavior of NSP Single Crystals. As an example of the impedance measurements, a Nyquist plot obtained at 23.5 °C is shown in Figure 3b; in Figure 3c, the temperature dependence of σ_{bulk} is presented. The Nyquist plot recorded at RT is composed by parts of a semicircle at high frequencies, followed by a sharp increase at low frequencies. This low frequency impedance can be attributed to the strongly ion blocking electrode and described by a resistance in parallel to a constant phase element (CPE_{el}) with the impedance given by $Z_{CPE} = 1/(i\omega)^n Q$, where ω is the angular frequency and the exponent n is a fit parameter accounting for nonideal behavior of the capacitance. It does not imply any mechanistic information, however, it is needed to analyze the sample-specific high frequency arc at higher temperatures. The high frequency part represents the bulk resistivity of the individual single crystals. The resistive part of the arc is approximated by a resistance element (R_{bulk}) and can be attributed to the volumetric Na-ion conduction σ_{bulk}, see below. The bulk capacitance (C_{bulk}) of the NSP samples cannot be obtained as we have to deal with an unavoidable and high stray capacitance C_{stray} in the order of 100 fF. The whole equivalent circuit used to analyze the impedance spectra is depicted in Figure 3b. The bulk (spreading) resistance between two circular microelectrodes with an electrode diameter d and bulk conductivity σ_{bulk} is given by $R_{bulk} = (d\sigma_{bulk})^{-1}$.[20] Here we obtain $\sigma_{bulk} = 3.04 \times 10^{-4}$ S cm^{-1} at RT; this value shows almost no variation within 20 measured single crystals, the error turned out to be less than 1%.

$\sigma_{bulk, lit.}$ (at 49 °C) is in almost perfect agreement with $\sigma_{bulk} = 1.70 \times 10^{-3}$ S cm^{-1} obtained in this study. Unfortunately, in ref 5, only activation energies E_a for the total conductivity are present from which we cannot access $E_{a, bulk}$. As can be seen in Figure 3c, the temperature dependence of σ_{bulk} of three randomly selected single crystals follows an almost perfect Arrhenius behavior according to $\sigma_{bulk}T = A \exp(-E_{a, bulk}/k_BT)$, where A is the pre-exponential factor of the ionic conductivity,

DOI: 10.1021/acs.chemmater.8b00179
Chem. Mater. 2018, 30, 1776−1781

and k_B denotes Boltzmann's constant. Up to 200 °C, no change in slope of $\sigma_{bulk}T$ versus $1000/T$ can be observed, for $E_{a,\ bulk}$ we obtain 0.39 eV. This analysis does not take into account that true temperatures at the sample surface are slightly lower than the set temperature due to asymmetric heating.

Hence, the true activation energy might be slightly larger that 0.39 eV. Our observation that no jumps of σ_{bulk} or changes in E_a occurred contrasts with earlier studies reporting up to two changes in the thermal activation of Na-ion conduction, see Figure 3d.

As shown in Figure 3d, Boehm et al. and Susman et al. (*idem*) reported a temperature dependency of the Na-ion conductivity with two discontinuities in the E_a caused by the $\alpha \rightarrow \beta$ (64 °C) and $\beta \rightarrow \gamma$ (166 °C) phase transition.[5,22] In contrast, Winand et al., Delmas et al., and Sorokin et al. observed an $\alpha \rightarrow \beta$ or $\beta \rightarrow \gamma$ phase transition.[20,23,24] The E_a values from literature and this study are summarized in Table 2.

Table 2. Bulk Na-Ion Conductivities (σ_{bulk}) and Activation Energies (E_a) of $Na_3Sc_2(PO_4)_3$ Single Crystals Compared to Literature Values for Polycrystalline Samples[a]

	E_a [eV]			
phase	α	β	γ	σ_{bulk} @49 °C [S cm^{-1}]
this study	0.39	0.39	1.70×10^{-3}	
Boehm[5]	0.56	0.45	0.15	1.25×10^{-3}
Delmas[20]		1.10	0.42	
Winand[22]	0.49	0.34		
Sorokin[23]		0.55	0.42	

[a]Since no σ_{bulk} values are reported in literature, we used the only available Nyquist plot of ref 5 to extract $\sigma_{bulk,\ lit.} = 1.25 \times 10^{-3}$ S cm^{-1} at 49 °C (see Table 2).

Unfortunately, in most of the previous experimental reports, only the final conductivity values are presented without providing details on the procedures how source data were analyzed. At least Boehm et al. and Sorokin et al. give some information about the inability to separate bulk and grain boundary contributions at temperatures above 50 °C. Their experimental setup was limited and only allowed impedance measurements up to 500 kHz, which seems to be too low to separate bulk electrical processes with fast relaxation rates. Consequently, they were restricted to use only total conductivities instead of bulk values to correlate Na-ion conductivity with structural changes.[5,24] Since the crystal chemistry of a material is usually correlated mainly to bulk properties, the use of overall conductivities could be misleading. In many cases, so far powders with μm-sized crystallites were considered and no nanostructured materials with disordered interfacial regions. Therefore, σ_{bulk} is then expected to exceed $\sigma_{g.b.}$; furthermore, we would anticipate $E_{a,\ bulk} < E_{a,\ g.b.}$. If σ_{total} represents a mixture of the two components with mutable contributions over the temperature range covered, slope changes in Arrhenius plots might be artificially generated. These changes might not show up if characteristic electric relaxation frequencies are used to evaluate conduction processes.

In our case, we did not find any convincing indications for a $\alpha \rightarrow \beta$ transition of NSP single crystals grown by the flux method. Hence, we do not expect a change in σ_{bulk} at temperatures below 120 °C. Indeed, the measured bulk conductivities simply follow a straight Arrhenius line (see Figures 3c and 3d). Importantly, the $\beta \rightarrow \gamma$ phase transition, for which we in fact find indications from DSC, has no measurable impact on σ_{bulk}. Up to 200 °C the pre-exponential factor A and $E_{a,\ bulk}$ remain unchanged. A point worth mentioning is that the space groups suggested for the β and γ phase, and even for the α form, are very similar. The structural changes only result from different Na-ion ordering.[4] Of course, order−disorder phenomena may easily influence configurational and vibrational entropy contributions of the pre-exponential factor. Also activation energies of local hopping processes can change and affect long-range ion transport. Here, as far as the bulk conductivity is concerned, we exclude any significant influence of the $\beta \rightarrow \gamma$ phase transition on σ_{bulk} of single-crystalline NSP. Finally, this finding agrees well with the singular result of Winand et al.,[23] see Figure 3d. Although they studied polycrystalline samples as others,[5,21−24] they analyzed impedance data[23] recorded up to 10 MHz instead of only 500 kHz (see above). In summary, on the basis of the microcontact impedance measurements σ_{bulk} is, if at all, only marginally influenced by the decreasing Na-ion ordering in NSP single crystals.

CONCLUSIONS

NSP single crystals were prepared by flux growth and investigated by SC XRD, MC IS, and DSC with respect to its crystal structure and Na-ion conduction as a function of temperature. SC XRD experiments in the suggested α (RT), β (130 °C), and γ phase (230 °C) regions identified at least two different modifications. The phases can be assigned to the β and γ modification, with *SG* $P\bar{3}cl$ and *SG* $R\bar{3}c$, respectively. From our data, we do not find clear indications of the α phase although superlattice peaks become more intense with decreasing temperature. Instead, DSC measurements point to a single phase transition at about 140 °C, which we assign to the $\beta \rightarrow \gamma$ phase transition; a possible $\alpha \rightarrow \beta$ transition remains invisible in our DSC and SC XRD measurements.

The $\beta \rightarrow \gamma$ transition does not lead to discontinuities of the Arrhenius behavior of $\sigma_{bulk}T$ of NSP single crystals when investigated with microcontact impedance spectroscopy. As far as ionic bulk properties are considered, this behavior is characterized by $\sigma_{bulk} = 3.04 \times 10^{-4}$ S cm^{-1} at RT $E_{a,\ bulk} = 0.39$ eV.

AUTHOR INFORMATION

Corresponding Author

*E-mail: rettenwander@tugraz.at.

ORCID

Daniel Rettenwander: 0000-0002-2074-941X

Martin Wilkening: 0000-0001-9706-4892

Author Contributions

The manuscript was written through contributions of all authors.

Funding

The research was supported by the Austrian Science Fund (FWF) Project No. P25702 and the Austrian Federal Ministry of Science, Research and Economy, and the National Foundation for Research, Technology, and Development.

Notes

The authors declare no competing financial interest.

REFERENCES

(1) Goodenough, J. B.; Hong, H. Y.-P.; Kafalas, J. A. Fast Na^+-ion transport in skeleton structures. *Mater. Res. Bull.* **1976**, *11*, 203−220.

DOI: 10.1021/acs.chemmater.8b00179
Chem. Mater. 2018, 30, 1776−1781

(2) Hong, Y.-P. Crystal structures and crystal chemistry in the system $Na_{1+x}Zr_2Si_xP_{3-x}O_{12}$. *Mater. Res. Bull.* **1976**, *11*, 173−179.
(3) Chotard, J.-N.; Rousse, G.; David, R.; Mentre, O.; Courty, M.; Masquelier, C. Discovery of a Sodium-Ordered Form of $Na_3V_2(PO_4)3$ below Ambient Temperature. *Chem. Mater.* **2015**, *27*, 5982−5987.
(4) Collin, G.; Comes, R.; Boilot, J. P.; Colomban, P. Disorder of tetrahedra in Nasicon-type structure—I.: $Na_3Sc_2(PO_4)_3$: Structures and ion-ion correlations. *J. Phys. Chem. Solids* **1986**, *47*, 843−854.
(5) Boehm, L.; Delbecq, C. J.; Hutchinson, E.; Susman, S. Fast ion conduction and phase transitions in various preparations of $Na_3Sc_2P_3O_{12}$. *Solid State Ionics* **1981**, *5*, 311−314.
(6) Boilot, J. P.; Collin, G.; Comes, R. Phase transition in Nasicon compounds $Na_3Sc_2P_3O_{12}$ and $Na_{1+x}Zr_2(P_{3-x}Si_x)O_{12}$. *Solid State Ionics* **1981**, *5*, 307−309.
(7) Delbecq, C. J.; Marshall, S. A.; Susman, S. Dielectric Properties of the Fast-Ion Conductor $Na_3Sc_2P_3O_{12}$. *Phys. Status Solidi B* **1981**, *106*, 731−734.
(8) Guin, M.; Dashjav, E.; Kumar, C. M. N.; Tietz, F.; Guillon, O. Investigation of crystal structure and ionic transport in a scandium-based NASICON material by neutron powder diffraction. *Solid State Sci.* **2017**, *67*, 30−36.
(9) Kim, Y.; Arunkumar, P.; Kim, B. Y.; Unithrattil, S. A zero-thermal-quenching phosphor. *Nat. Mater.* **2017**, *16*, 543−550.
(10) Moon, S.-H.; Kim, Y. H.; Cho, D.-C.; Shin, E.-C.; Lee, D.; Im, W. B.; Lee, J.-S. Sodium ion transport in polymorphic scandium NASICON analog $Na_3Sc_2(PO_4)_3$ with new dielectric spectroscopy approach for current-constriction effects. *Solid State Ionics* **2016**, *289*, 55−71.
(11) Wang, X. C.; Zhao, Z. Y.; Wu, Q. S.; Wang, C.; Wang, Q.; Li, Y. Y.; Wang, Y. H. Structure, photoluminescence and abnormal thermal quenching behavior of Eu^{2+}-doped $Na_3Sc_2(PO_4)_3$: a novel blue-emitting phosphor for n-UV LEDs. *J. Mater. Chem. C* **2016**, *4*, 8795−8801.
(12) Tran Qui, D.; Capponi, J. J.; Gondrand, M.; Joubert, J. C. Relation between crystal structure and ionic conductivity for $Na_{3(1+x)}Sc_{2-x}(PO_4)_3$. *Solid State Ionics* **1981**, *5*, 305−306.
(13) Collin, G.; Comes, R.; Boilot, J. P.; Colomban, P. Nasicon analog $Na_3Sc_2(PO_4)_3$: Thermal behaviour of the α, β and γ types, structure, correlations and transitions. *Solid State Ionics* **1988**, *28*, 437−441.
(14) Rettenwander, D.; Welzl, A.; Pristat, S.; Tietz, F.; Taibl, S.; Redhammer, G. J.; Fleig, J. A microcontact impedance study on NASICON-type $Li_{1+x}Al_xTi_{2-x}(PO_4)_3$ ($0 \leq x \leq 0.5$) single crystals. *J. Mater. Chem. A* **2016**, *4*, 1506−1513.
(15) Sotofte, I.; Fu, D. C. Redetermination of the crystal structure of $Na_3Sc_2(PO_4)_3$. *Solid State Ionics* **1988**, *26*, 307−310.
(16) Bruker. *APEX3 (Version 2015. 10−0)*; Bruker AXS Inc: Madison, WI, 2015.
(17) Stoe & Cie. *X-AREA and X-RED32*; Stoe & Cie: Darmstadt, Germany, 2006.
(18) Ditmars, D. A.; Ishihara, S.; Chang, S. S.; Bernstein, G. M.; West, E. D. Measurements of the relative enthalpy of pure α-Al2O3 (NBS heat capacity and enthalpy standard reference material no. 720) from 10 to 1,950 K. *J. Res. Natl. Bur. Stand.* **1982**, *87*, 5−9.
(19) Redhammer, G. J.; Ende, M.; Effenberger, H.; Lengauer, C.; Rettenwander, D.; Guin, M.; Tietz, F.; Miletich, R.; Crystal structure of $Na_3Sc_2(PO_4)_3$ between 90 and 500 K, *in preparation*.
(20) Newman, J. Resistance for Flow of Current to a Disk. *J. Electrochem. Soc.* **1966**, *113*, 501−502.
(21) Delmas, C.; Viala, J. C.; Olazcuaga, R.; Le Flem, G.; Hagenmuller, P.; Cherkaoui, F.; Brochu, R. Conductivite ionique dans les systems $Na_{1+x}Zr_{2-x}L_x(PO_4)_3$ (L = Cr, Yb). *Mater. Res. Bull.* **1981**, *16*, 83−90.
(22) Susman, S.; Delbecq, C. J.; Brun, T. O.; Prince, E. Fast ion transport in the NASICON analog $Na_3Sc_2(PO_4)_3$: Structure and conductivity. *Solid State Ionics* **1983**, *9-10*, 839−844.
(23) Winand, J. M.; Rulmont, A.; Tarte, P. Ionic conductivity of the $N_{a1+x}M_x^{III}Zr_{2-x}(PO_4)_3$ systems (M = Al, Ga, Cr, Fe, Sc, In, Y, Yb). *J. Mater. Sci.* **1990**, *25*, 4008−4013.
(24) Sorokin, N. I. Na+-ion conductivity of double phosphate $Na_3Sc_2(PO_4)_3$ in the region of the β-γ transition. *Phys. Solid State* **2014**, *56*, 678−681.

DOI: 10.1021/acs.chemmater.8b00179
Chem. Mater. 2018, 30, 1776−1781